Contents lists available at ScienceDirect

Advanced Powder Technology

journal homepage: www.elsevier.com/locate/apt

Original Research Paper

Effect of milling time on structural, physical and tribological behavior of a newly developed Ti-Nb-Zr alloy for biomedical applications

Fouzia Hamadi [a,b,*], Mamoun Fellah [b,c,*], Naouel Hezil [a,b], Dikra Bouras [d], Salah Eddine Laouini [e], Alex montagne [f], Hamiden Abd El-Wahed Khalifa [g,h], Aleksei Obrosov [i], Gamal A. El-Hiti [j], Krishna Kumar Yadav [k,l]

[a] Matter Sciences Department, ABBES Laghrour – Khenchela University, 40004, Algeria
[b] Biomaterial, Synthesis and Tribology Research Team, Khenchela University, 40004, Algeria
[c] Mechanical Engineering Department, Khenchela University, 40004, Algeria
[d] Faculty of Science and Technology, University of Souk-Ahras, Algeria
[e] Laboratory of Biotechnology Biomaterials and Condensed Matter, Faculty of Technology, University of El Oued, El Oued 39000, Algeria
[f] Université Polytechnique Hauts-de-France, LAMIH UMR 8201, F-59313 Valenciennes, France
[g] Department of Mathematics, College of Science and Arts, Qassim University, Al-Badaya 51951, Saudi Arabia
[h] Department of Operations and Management Research, Faculty of Graduate Studies of Statistical Research, Cairo University, Giza 12613, Egypt
[i] Brandenburg University of Technology Cottbus-Senftenberg, 03046 Cottbus, Germany
[j] Department of Optometry, College of Applied Medical Sciences, King Saud University, Riyadh 11433, Saudi Arabia
[k] Faculty of Science and Technology, Madhyanchal Professional University, Ratibad, Bhopal 462044, India
[l] Environmental and Atmospheric Sciences Research Group, Scientific Research Center, Al-Ayen University, Thi-Qar, Nasiriyah 64001, Iraq

ARTICLE INFO

ABSTRACT

Titanium (Ti)-based alloys with only a β-phase have attracted academic and industrial interest for orthopedic application, due to their close properties to those of tissues. The current study aims to investigate the effect of milling time (2 h, 6 h, 12 h and 18 h) on the nanostructured ternary alloy Ti-25Nb-25Zr prepared by high energy milling, on its structural, physical and tribological behaviors. The alloys' characteristics such as relative density/porosity, surface roughness, were evaluated using XRD, SEM, surface profilometry, and microdurometer, respectively. The tribological characterization was done using an oscillating tribometer under wet conditions, simulating the human body environment. Results showed that the crystallite and mean pore size reduced with increasing milling time, with the smallest values of 26 nm and 40 μm, respectively after 18 h. Structural characterization shows that the amount of the β-Ti phase increased with increasing milling time, resulting in spherical morphology and texturing of the synthesized alloys. The milled alloys' structural evolution and morphological changes were sensitive to their milling times. Also, the relative density, Young's modulus and hardness, increased due to grain size decreased with increasing milling time. Tribological results showed that the effect of milling has a significant effect on both nanomaterial formation and friction-wear behavior of the alloys. The results showed that, friction coefficient and wear rate significantly decreased due to the increased formation of protective films such as TiO_2, Nb_2O_5 and ZrO_2 phases. The wear mechanism of the Ti-25Zr-25Nb system was dominated by abrasion wear accompanied by adhesion wear.

1. Introduction

Ti is the 9th most element on Earth (0.44–0.6 % of the earth's crust, according to estimates) and ranks 4th in the list of metals after iron, aluminum and magnesium [1]. It has many industrial applications and is widely used in the biomedical field. It is a material of choice for implantology, because of its excellent biocompatibility and its mechanical properties. That's why it constitutes a major part of an implant [2].

By mixing titanium with other elements, different crystalline structures are obtained that can be stabilized at room temperature and enable to manufacture 3 types of Ti-alloys: α-alloys, β-alloys and α + β alloys [3]. Among all the Ti-alloys, the Ti-6Al-4 V two-

* Corresponding authors at: a. Matter Sciences Department, ABBES Laghrour – University, Khenchela, 40004, Algeria. b. Biomaterial, Synthesis and Tribology Research Team, Abbes Laghrour university- Khenchela, 40004, Algeria.
E-mail addresses: fouzia_hammadi@univ-khenchela.dz (F. Hamadi), mamoune.fellah@univ-khenchela.dz (M. Fellah).

phases alloy, initially developed for the aeronautical sector is the most widely used.

The main elements that can be added to titanium are classified into two categories: beta and alphagenic elements. The beta elements decrease the transus while the alpha elements increase it [4]. Given the important and positive role of some elements, their presence affects mechanical and tribological properties, either through solid solutions of substitution or insertion, or by modifying morphology [5]. Alphagenic elements (H, C, B, and N) are non-metallic elements found only in insertion, due to their smaller size compared to metallic elements. Betagenic elements are found only in substitution [6]. For example, molybdenum (Mo) improves strength, ductility and creep at medium temperatures. It also increases resistance to oxidation [7]. The addition of vanadium (V) improves ductility, thereby helping to make the material more flexible [8]. However, alternatively, the presence of vanadium decreases the oxidation resistance of the material. Chromium (Cr) plays a similar role to that of molybdenum by improving strength but decreasing ductility [9,10].

Furthermore, Zr improves the strength-ductility-creep compromise at medium temperature (it reduces the temperature of transus making it feasible to work at lower temperatures), it increases the hot cracking resistance and reduces the tendency of the alloy to stick or weld to the walls of the mold [11]. However, an increase in the milling time is normally accompanied by a reduction in ductility, while silicon (Si) improves creep resistance due to precipitation [12]. All these additional elements can be added to titanium, in larger quantities, to produce a titanium alloy whose properties are optimized to suit the desired application (implantology, aerospace, armaments, aeronautics…) [13].

The most promising alloys include Ti-13Nb-13Zr and Ti-12Mo-6Zr-2Fe, which have been authorized by the FDA [14,15]. Titanium (Ti)-based alloys with only a β-phase have attracted academic and industrial interest for orthopedic application, due to their close properties to those of tissues. Other research have also shown that the elastic modulus of milled Ti-Nb-Zr alloys attained ≈55 GPa, which is comparable to the bone young's modulus as reported in the literature [16,17]. The Ti-35Zr-28Nb alloy was composed of a single β-phase [16,17].

Moreover, a lower wear volume and COF with high wear resistance are important for biomaterials to reduce the release of metallic ions and the formation of wear debris, which can trigger undesirable body reactions [18]. Some researchers indicated that the wear behavior of the Ti-Zr-Nb is better than that of the pure Ti [15]. Thanks to their excellent biocompatibility and corrosion resistance, Ti-Zr-Nb alloys also have the ability to osseointegrate, i.e. fuse stably with surrounding bone tissues. This promotes healing and bone growth around the implant, providing strong and long-lasting fixation. This osseointegration capability is particularly important in orthopedic and dental applications, where strong integration between implant and bone is essential to ensure long-term stability and functionality [19].

During the ball milling process, some alloy elements such as Nb, Zr and Mg underwent softening. This softening caused a phase transformation in the Ti crystal structure, leading to the formation of the Ti-β phase. [15]. Furthermore, most of the previous studies do not take into account the milling time effect on the different behavior of mechanically alloyed Ti-25Nb-25Zr alloys. Zr, Nb and Ti, are biocompatible, non-allergenic and non-toxic metals, and the addition of Zr and Nb to Ti favors the mechanical biocompatibility between the bone and the alloy [20,21]. Hence, the aim of this paper is to investigate for the first time, the effect of milling time and elemental content on the microstructural evolution, tribological and mechanical behaviors of Ti-25Nb-25Zr alloy.

2. Materials and methods

2.1. Samples preparation

2.1.1. Materials and synthesis

The materials used were all of analytical purity. For the fabrication of the nanomaterials, titanium (Ti) was supplied by Allegheny Technologies Incorporated (ATI) in Pittsburgh, Pennsylvania, USA, while zirconium (Zr) and niobium (Nb) were supplied by H.C. Starck (Global Advanced Metals, USA). Fig. 1 shows the typical shape of the elemental powders, which had a particle size of 20 μm. Mechanical alloying was carried out in a steel tank utilizing a planetary ball mill (Pulverisette, Fritsch P7), under Ar gas as shielding gas to reduce the particle size of the initial powders in the range of 10 to 100 μm. The milling was done in dry medium at a flask speed of 450 rpm. The pure powders in the Ti-25Nb-25Zr weight composition were milled for different periods of 2, 6, 12, and 18 h respectively with a balls-to-powder ratio (BPR) of 15:1.

A mandatory 10 min break, after 20 min of milling was given in order to avoid high temperatures inside the vials during milling [22]. After milling the Ti, Nb and Zr elemental powders, their structural and microstructural properties were investigated using several methods such as XRD and SEM with EDS.

The Ti-Nb-Zr system with 25 (wt.%) of both Zr and Nb elements leads to the formation of Ti-25Nb-25Zr alloy with a structure that contains only β phase according to the ternary diagram of Ti-Nb–Zr
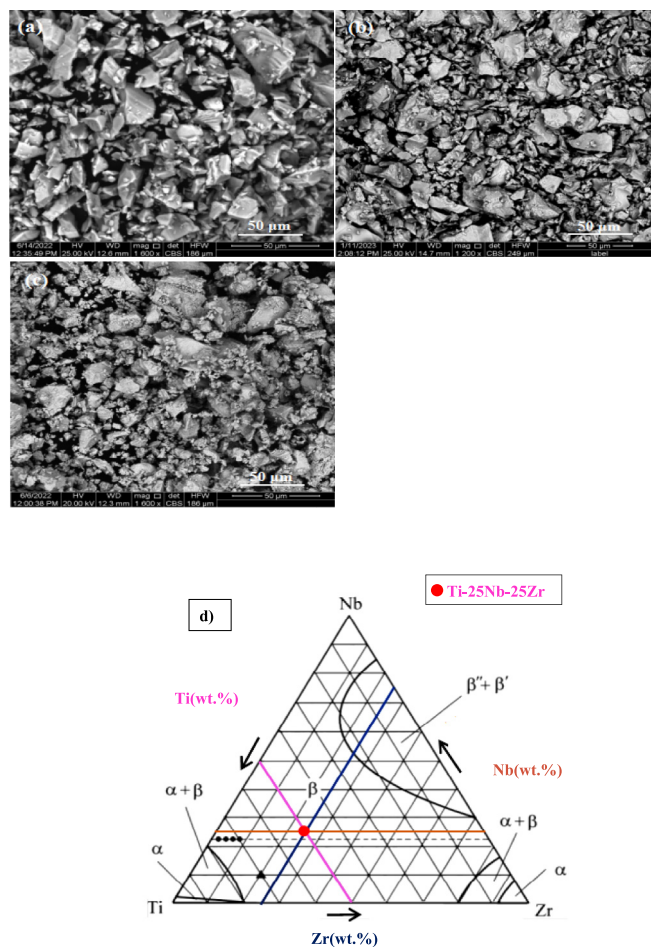

Fig. 1. SEM image of starting powders of: a) Ti, b) Nb, c) Zr. d) Ternary diagram of the Ti-25Nb-25Zr system obtained at 1150 °C [43].

system (Fig-1.d). Generally, all biomaterials' alloys containing Zr, Nb and Ti displayed a "near" β-phase. On the other hand, for Ti–27Nb–13Zr, an increase in milling time exhibited an increase in the α'' phase [23,24].

There is more β-Ti e than α-Ti phas in alloys prepared with powder milled for 2 h and 6 h. An increase in milling time to 12 h resulted in an equiaxed structure with α colonies and α-plates in the β matrix, and all the niobium was in solution. Following the formation of Ti alloy nanoparticles, densification techniques were applied, followed by sintering to improve mechanical and tribological properties: cold uniaxial compaction under a fixed pressure of 300 MPa using a hydraulic press, then HIPed and sintering at 3×10^{-6} mbar for 3 h at a of 1250 °C [22]. The properties of as-received starting powders are shown in Table 1.

Fig. 2 shows the sintering cycle of the pellets.

2.2. Materials characterization

Fig. 3 illustrates the framework of this research and the experimental procedure used in this work along with the characterization techniques used to interpret the data.

2.2.1. Structural characterization

Phase identification was performed by XRD, with CuKα radiation (λ = 1.5407 Å) operated in a 2θ range of 10°–90° at a speed of 2° /min. Analysis by scanning electron microscopy (QUANTA 250, FET.), associated with microanalysis by dispersive energy of X-rays (SEM-EDX) was carried out to determine the microstructure, the chemical composition and the morphology of the milled powders.

The nanocrystallite size was estimated by measuring the peak broadening at the point where the diffraction intensity reached half of its maximum value (FWHM) on the most intense peak (2θ = 40° on the face (101)) and then applying Scherer's equation [25].

$$L = \frac{K\lambda}{\beta \cos\theta} \tag{1}$$

From the XRD models, the lattice parameters, were estimated using the following equations:

- In the case of a cubic structure, the lattice parameter is linked to the Miller indices and to the inter-reticular distance by the equation (2):

$$d_{hkl} = \frac{a}{\sqrt{\left(h^2 + k^2 + l^2\right)}} \tag{2}$$

- In the case of a compact hexagonal structure, the lattice parameter is related to the Miller indices and to the inter-reticular distance by the equation (3):

$$d_{hkl} = \frac{a\sqrt{3}}{2} \frac{1}{\sqrt{\left((h^2 + k^2 + h.k + \frac{3}{4} \cdot \frac{a^2}{c^2} \cdot l^2)\right)}} \tag{3}$$

2.2.2. Mechanical characterization

In order to assess the mechanical properties, the samples were subjected to hardness measurements. These tests were conducted using a Vickers diamond indenter (Zwick ZHV0.05) with a load of 50 mN and a dwell time of 10 s. The Vickers hardness values reported are the mean of a minimum of three measurements taken for each alloy composition.

2.2.3. Tribological characterization

Tribological characteristics were assessed under wet conditions using a PBS solution, the composition of which is given in Table 2, using a multifunctional friction and wear tester. The specimens used for the friction and wear tests had a surface area of 10 mm x 5 mm and were slid against a 6 mm (Fig. 4) diameter alumina (Al_2O_3) ball. The testing time was 30 min, using varying normal loads (2–20 N), with a sliding distance of 1000 m and a velocity of 15 mm/s. Trace length was 5 mm. (i.e. 10 mm round trip). The reciprocating frequency was 5 Hz and 10 Hz.

During wear tests, coefficient of friction (COF) was determined by dividing frictional force (F_f) by normal force (F_n) [26].

$$COF = \frac{F_f}{F_n} \tag{4}$$

The loss of material was evaluated by measuring the decrease in volume from the dimensions of the wear mark, using an optical profiler. Each test was repeated four times to ensure the results accurateness. The surfaces of the counter body were polished to obtain a smooth and uniform texture. Particular attention has been paid to controlling and treating the wear track region before and after each experiment, to ensure reproducibility of results between tests.

The equation used to calculate the wear rates of all specimens was as follows:

$$W_r = \frac{V}{P.L} \tag{5}$$

The wear rate W_r is calculated based on the wear volume (V) in mm³, the applied load (P) in N and the total sliding distance (L). The surface profiles were investigated using a 3D profilometer (Alti Surf 500).

3. Results and discussion

3.1. Structural characterization

3.1.1. Powders morphology

Fig. 5 represents the morphology of Ti-25Nb-25Zr powder after mechanical alloying. The particle size initially increased and then decreased, which corresponds to the general characteristics of the mechanical alloying process [27].

The particle size scattering and the agglomerate structure visible in the microphotographs confirm the fracturing and the continuous cold welding of starting powders. The majority of rounded

Table 1
Properties of as-received powders [22].

| Characteristic	Ti	Nb	Zr
Purity	> 99.9 %		
Particle size(wt.%)	<100 μm		
O(wt.%)	0.057	0.315	0.213
Fe(wt.%)	0.0054	0.00033	0.0003
N(wt.%)	0.0015	0.0015	0.00331
H(wt.%)	0.006	0.00024	0.00089
C(wt.%)	0.03	0.0075	0.002
Phase at STP	Solid		
Atomic radius (nm)	0.147	0.143	0.160
Crystal system	(hcp)	(bcc)	(hcp)
Melting temperature (°C)	1674	2478	1854
Morphology	The particles are irregular in shape		
Density (g/cm³)	4.5	8.57	α-phase 6.50
			β-phase 6.05
Composition (Wt.%)	Balance	25.1	24.8
Fabrication process	Chemical process		
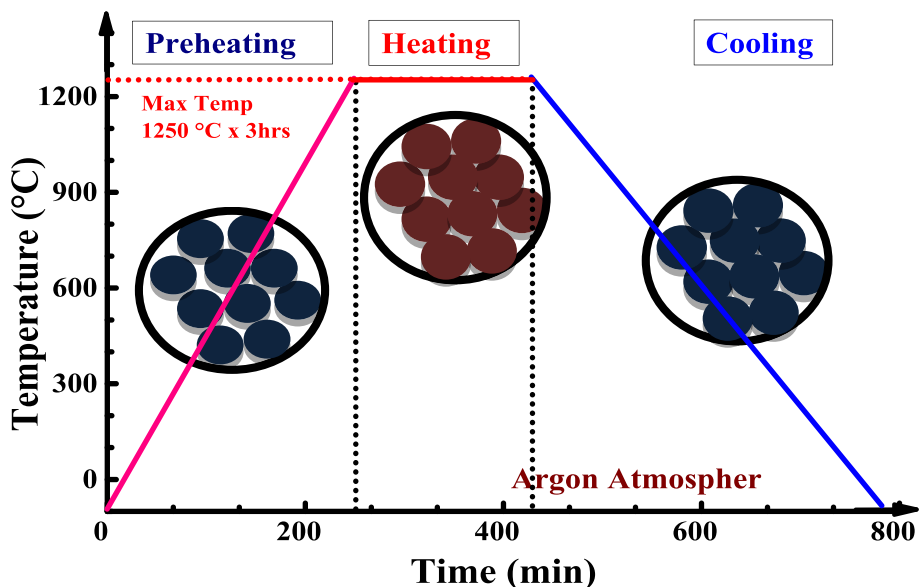
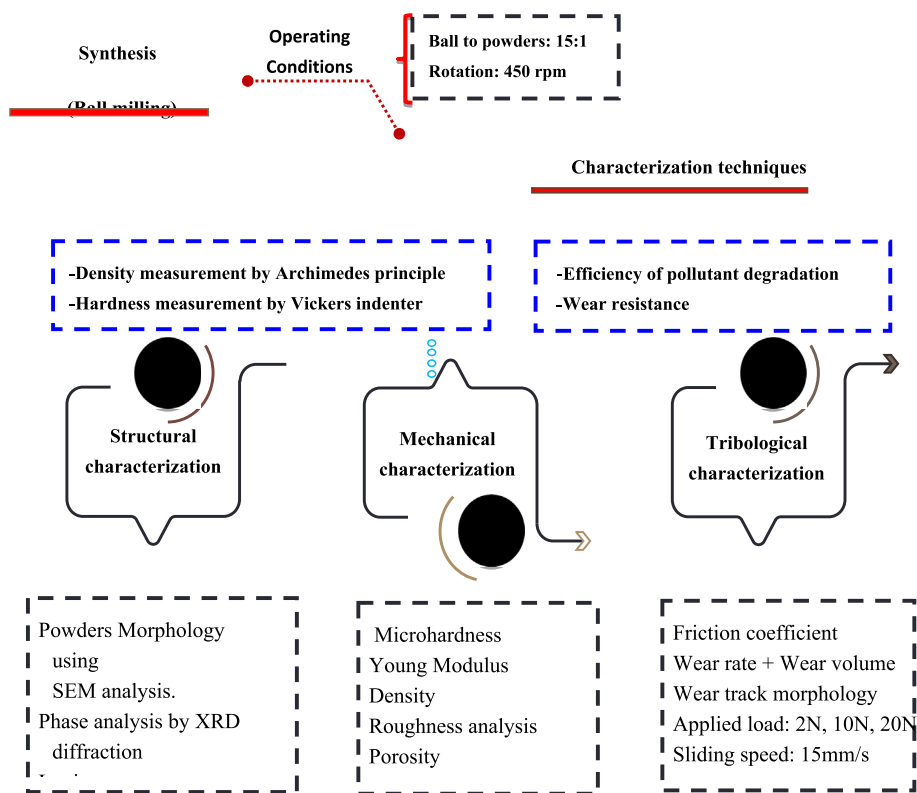**Fig. 2.** Sintering process of milled Ti-25Nb-25Zr alloys.

Fig. 3. Sample preparation process and characterization techniques.

Table 2
Chemical composition of PBS solution [25].

Compounds	NaCl	KCl	Na$_2$HPO$_4$	K$_2$HPO$_4$
Concentration (M)	0.14	0.0028	0.008	0.002

agglomerated particles are between 10 and 100 µm in size [28]. The milled powder was observed to be composed of several nanoparticles, due to the repeated collisions of the balls and extrusion, resulting in the metal powder being continuously plasticized, hardened, cold-welded, and broken [27].

Table 3 shows the EDS analysis of Ti-25Nb-25Zr for 2 and 18 h of milling time. After 2 h of milling, no presence of contamination elements is detected, only the alloy composition is observed (Ti, Nb, and Zr). But for alloys milled during 18 h, the EDS analysis
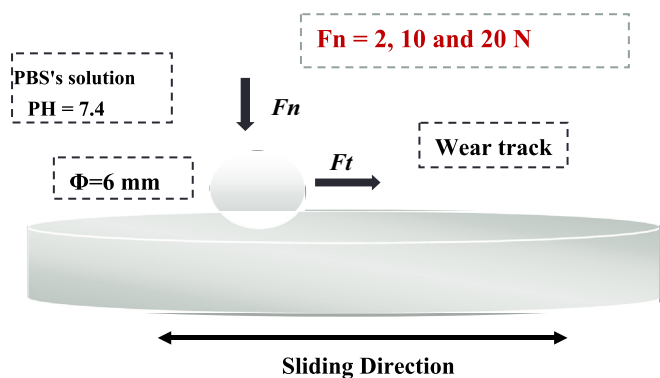
Fig. 4. Schema of Tribotester (TRIBOtechnic type ball-on-disc).

3.1.2. XRD analysis

As revealed in Fig. 6, the peak intensity reduced and became broadened as increasing the milling time from 2 to 18 h. The diffraction peak of the initial Ti-25Nb-25Zr powder can be indexed to Ti, Zr and Nb, and the characteristic (*hkl*) lines of these elements are only visible after 15 min of milling [20,17,31,32]. There were visible peaks after 2 h of milling and a mixture of the elements was formed during the first stage of mechanical alloying. The intensity of the Zr and Nb peaks decreased over time. Peaks from Nb were close to β-Ti, and the intensity appeared to decrease slowly [10].

Though, the diffraction peaks of Ti-25Nb-25Zr powder are significantly enlargement and even misplaced after 18 h of milling (Fig. 6), indicating the formation of metastable β-phase by mechanical alloying. A similar tendency has also been observed from XRD analysis for the Ti-Zr-Nb-Mo systems [17,20,33,34].

3.1.3. Lattice parameters

To determine the microstrain, we used the Williamson-Hall equation, which relates the width at half maximum of the diffraction peaks to the microstrain. (Fig. 7).

Fig. 8 illustrated the variation of mean lattice parameters, crystallite size and microstrain of Ti-25Nb-25Zr alloy as function of milling times.

Fig. 8a illustrates the evolution of mean crystallite size of Ti-25Nb-25Zr. As can be seen for milling time from 2 to 12 h, the mean crystallite size revealed a decrease from 53 to 26 nm. For samples
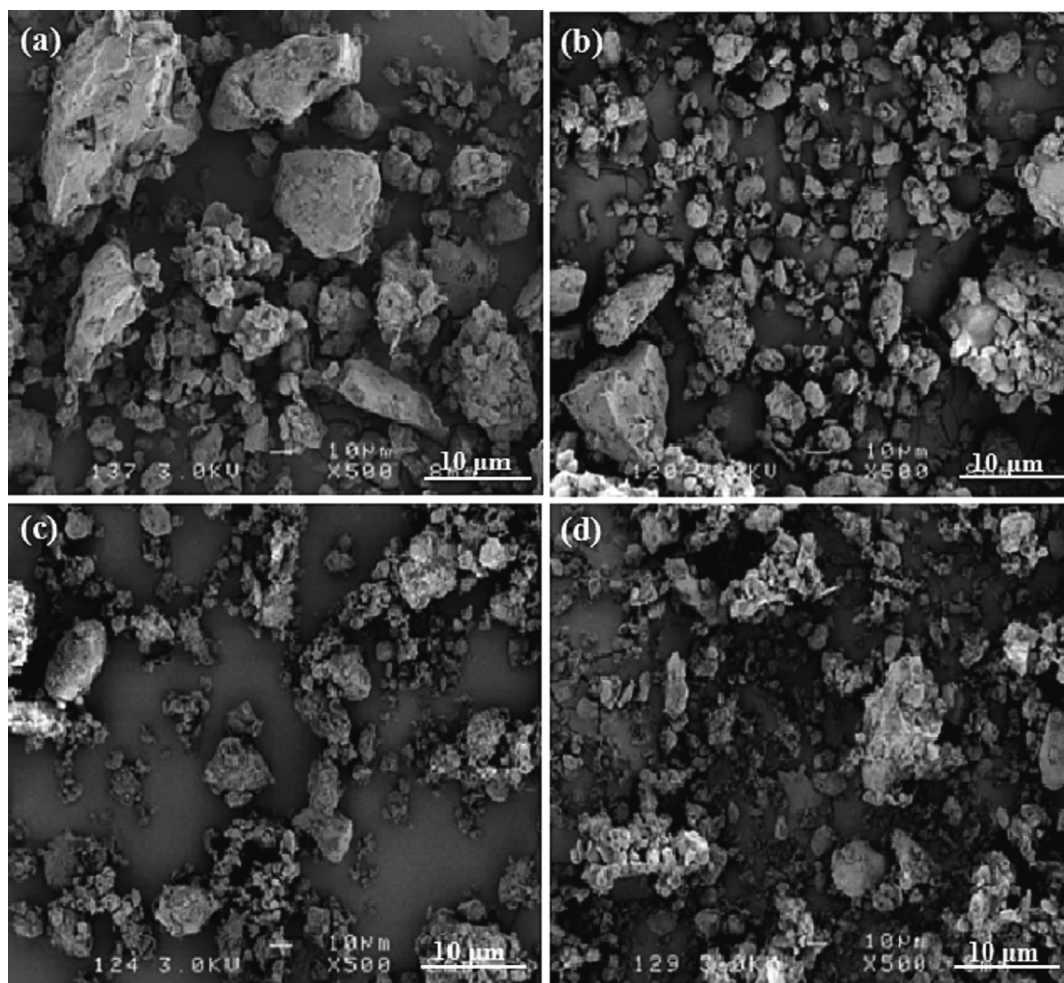
revealed the presence of Si and O from alumina balls, vials and atmosphere. The EDS analysis showed an increase in contaminants at a higher time of milling. Previous research has shown that, due to the impact of grinding bodies, powder may be contaminated with the container material because the material can break off and become incorporated into the powder; leading to the chemical composition change of the powder [29,30].
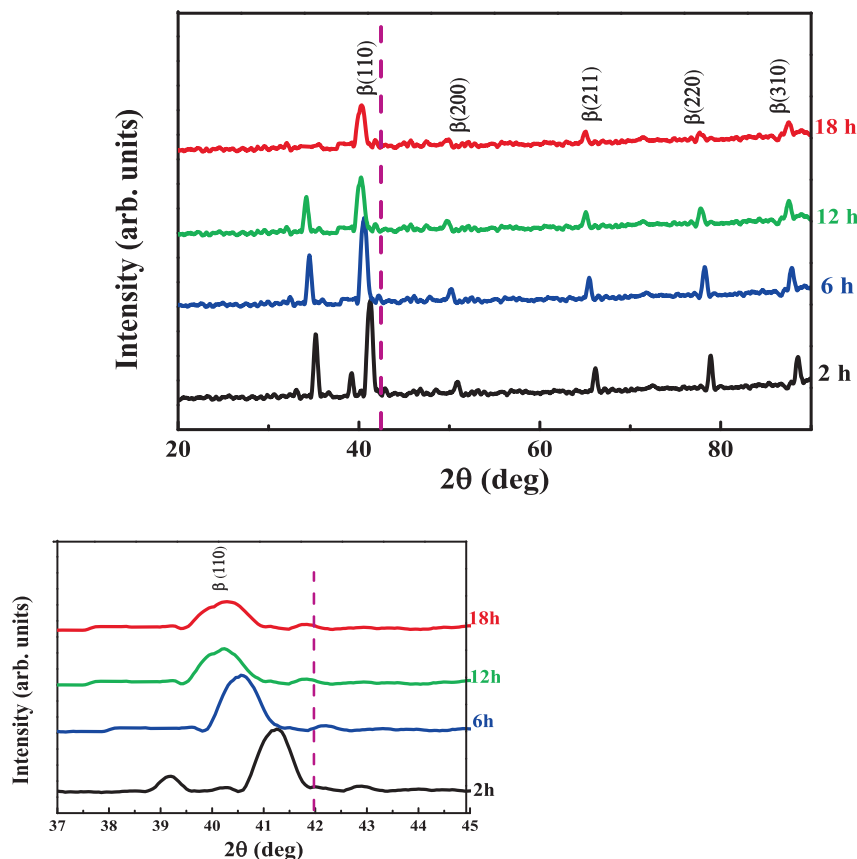

Fig. 5. SEM micrograph of Ti-25Nb-25Zr powder milled for: a) – 2 h, b)-6h; c)-12 h and d)-18 h.

Table 3

EDS analysis of Ti-25Nb-25Zr milled powders.

Milling time (h)	Ti(wt.%))	Nb(wt.%)	Zr(wt.%)	O(wt.%)	Si(wt.%)
2 h	47.5	27	24	1	0.5
6 h	44.0	26	28	2	0.03
12 h	46.7	26	24	3	0.3
18 h	44.8	25	26	4	0.2

Fig. 6. XRD patterns of Ti-25Nb-25Zr alloy after mechanical alloying during diverse milling time.

milled at 12 h and 18 h, the crystallite size decreases with milling time. This crystallite size decrease is primarily due to severe powder deformation [35]. With ongoing deformation, the particles harden, and fracture happened through a fatigue mechanism [36–38].

The structure of the particles is continuously refined due to the continuous action of the grinding bodies, but the particle size remains constant. As a result the interlamellar distances reduce and the number of lamellar structures in each nanoparticle increases [37–39]. Even though that large particles are typically smaller in size. The interlamellar distance decreases over time, and the size of the crystallites (or grains) is refined to nanometric dimensions [39,40]. Another explanation is that higher defect densities increase the possibility of nucleation sites during crystallization [40].

The changes in the obtained microstrain {ε} are also recorded in Fig. 8a. A significant increase in microstrain can be observed up to a value of 0.94 % with increasing milling time. This could be due to a high density of dislocation and a high concentration of stacking defects [40]. The powders are almost amorphous after 48 h of mechanical alloying. This has also been previously shown in [25]. Also, as previously confirmed, an increase in microstrain is associ-

ated to a decrease in the size of crystallite, which is consistent with the current study [40,41].

The Fig. 8.b displayed the evolution of Ti-25Nb-25Zr lattice parameters < a> (Å). The a_β lattice parameter increases from 3.153 to 3.212 Å as milling time increases. The Ti-25Nb-25Zr alloy with a milling time of 18 h has the highest lattice parameter due to the plastic deformation of powder particles resulting in a variety of defects including dislocations, stacking faults, and vacancies.

The presence of several atoms with different atomic sizes (Ti: r_{Ti} = 0.1472 nm, Zr: r_{Zr} = 0.1603 nm and Nb: r_{Nb} = 0.1434 nm) [20] creates tensions and deformations in the crystal lattice, disrupting its regular structure. These disturbances can cause distortions which are amplified by atomic interactions. Additionally, these distortions can also affect the lattice of the Ti-Nb-Zr alloy, thereby leading to an increase in the lattice parameters.
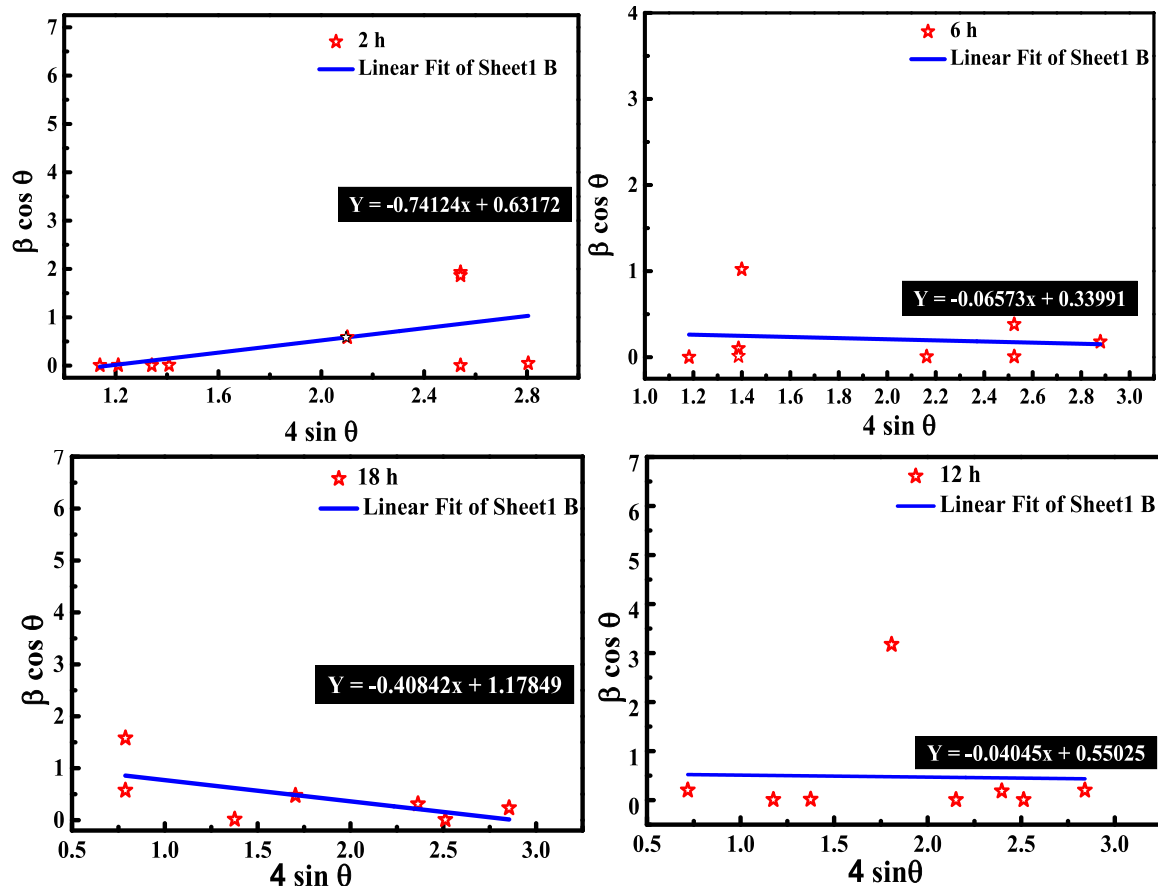
Fig. 7. Microstrain calculated using Williamson-Hall equation as function.

3.2. Physical and mechanical characterization

3.2.1. Porosity measurement

Fig. 9 represents the evolution of the porosity frequency of Ti-25Nb-25Zr. The variation is in the frequency of pore size ranges from 10 to 100 μm. Pore size was reduced to less than 100 μm due to the cold-welding process over particle fracture. This is due to particles sizes, which were smaller and more uniform in size than the starting powders [14].

During the first milling stage from 2 to 6 h, 73 % of the pores have a size of more than 70 μm. For ternary samples milled from 12 to 18 h, it was observed that samples had from 10 to 7 % of pores with a size higher than 70 μm, [41].

Fig. 10a indicates that mean pore size of Ti-25Nb-25Zr decreased with increasing milling time (2–18 h) from 66 μm to 40 μm respectively. This is due to the grain size refinement during the mechanical alloying process. However, for even longer grinding times, larger pores are observed due to pore agglomeration [41], and they are in agreement with a previous research [42].

The porosity level in nanomaterials is highly dependent on the processing technique used for mechanically alloyed specimens. The pore size can be smaller than or equal to the grain size even after agglomeration. Porosity and mean pore size have an important impact on the mechanical properties of nanomaterials [43]. As shown in Fig. 10.b, the relative porosity of sintered samples decreases from 22 to 13 % with increasing milling time. Conversely, the relative density (%) of the Ti–25Nb–25Zr alloys increased with the increased milling time. The sample milled at 18 h had the highest sintered density of 87 % and a relative porosity of 13 %.

These results are explained by a decrease in pore size due to the predominance of particle fracture in the cold welding process [39], an increase in closed porosity, and a decrease in open porosity [44]. In addition, the particles were smaller and more uniform in size than the starting powders. The Ti-35Zr-28Nb alloy is almost completely dense, they displayed uniform microstructures of a single β phase, and high relative density can be obtained by sintering [16].

3.2.2. Hardness and Young's modulus analysis

The Vickers hardness $HV_{0.05}$ and the Young's modulus E of Ti-25Nb-25Zr samples after 2 to 18 h milling are shown in Fig. 11a. The highest value of 350 $HV_{0.05}$ and the lowest value of 208 $HV_{0.05}$ were obtained after 18 h and 2 h of milling time, respectively [18].

The young's modulus of the ternary alloys increased from 92 GPa to 107 GPa with increasing milling times similarly to hardness [42].

The mechanical properties are highly influenced by the pore size and distribution. Furthermore, chemical composition and grain size are the main factors that can affect the mechanical properties of alloys (hardness and Young modulus) [15,45].

Fig. 11b represents H^3/E^2 and H/E ratios of Ti-25Nb-25Zr alloys as a function of milling time. It is observed that H/E values increase from 0.022 at 2 h of milling to 0.034 at 12 h of milling, and then decrease to 0.032 at 18 h of milling time. This change shows that with the increase in milling time, the wear resistance of the alloy increases first and then decreases. In fact, the Ti-25Nb-25Zr alloy milled for 12 h has the highest H/E value (0.034), indicating that the alloy is resistant to wear [46,47].
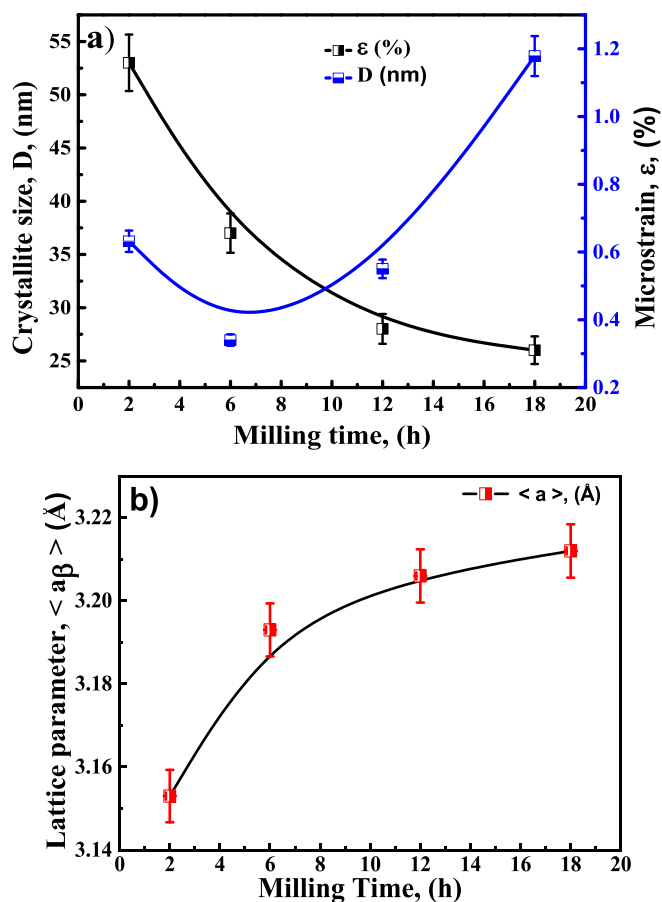
Fig. 8. Evolution of: a) Crystallite sizes and microstrain. b) Lattice parameters <a$_\beta$> of Ti-25Nb-25Zr samples.

One other inducator (H^3/E^2) implies plastic deformation resistance; the higher the value of H^3/E^2, the greater the resistance to plastic deformation [46–48]. Because wear is the progressive loss of material resulting from plastic deformation, this H^3/E^2 indicator could reveal a material's anti-wear ability [23,49–51]. Indeed, the high value of H^3/E^2 indicates a long service life [46–49]. The evolution of H3/E2 values is the same as for H/E values. The H3/E2 values increase from 0.0010 GPa to 0.0039 GPa from 2 h to 12 h of milling time respectively and then decrease to 0.0035 GPa at 18 h of milling time. Therefore, the Ti-25Nb-25Zr (milled at 12 h) with the highest H3/E2 value indicates the improved of its wear behaviour.

In addition, the H/E and the H^3/E^2 values of Ti-Nb-Zr alloys milled at 6 h, 12 h and 18 are close to those of Ti- alloys and are higher to Cp-Ti alloys (0.024 and 0.0014GPa respectively) [46,48].

3.2.3. Surface roughness analysis

A decrease in roughness Ra (Fig. 12) is noted as a function of milling time. For 2 h milling Ra is equal to 9.1 nm and at 6 h is equal to 8.0 nm, for 12 h equal to 7.6 and 7.10 nm for 18 h milling. It is well-known that the surface roughness of a material increases with the coefficient of friction during mechanical machining. This is expected since, in the case of a dry contact between metallic surfaces, the friction mechanism is based on plasticity. Consequently, a smaller real contact area and higher local pressures at asperity contacts are the consequences of greater roughness. This leads to a lower friction coefficient due to the decrease in the ability of these micro-contacts to bear the extra tangential load before sliding occurs. Moreover, the roughness of the material ensures better grip [50]. The results show that the roughness decreased as milling time increasing, up to a value of 7 nm at milling times of 18 h. According to the literature, this can increase the number of cells adhering to the substrate as well as the activity of cell [51].
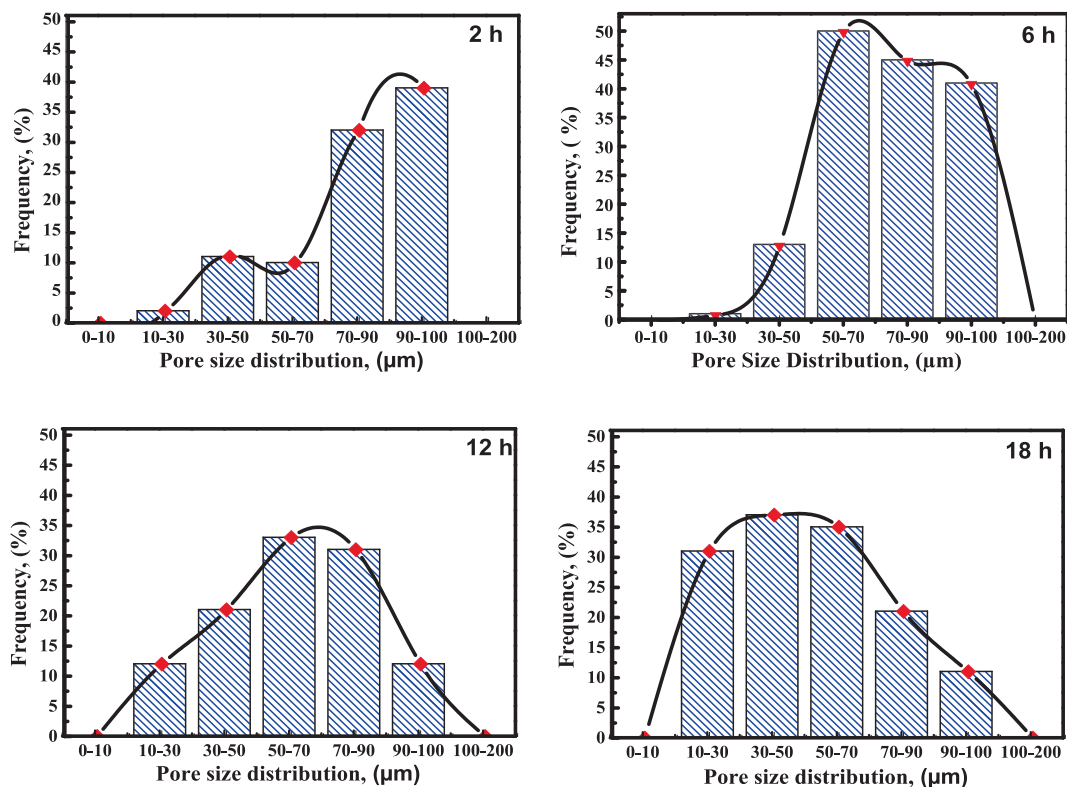

Fig. 9. PSD frequency of Ti-25Nb-25Zr milled samples as function of milling times.
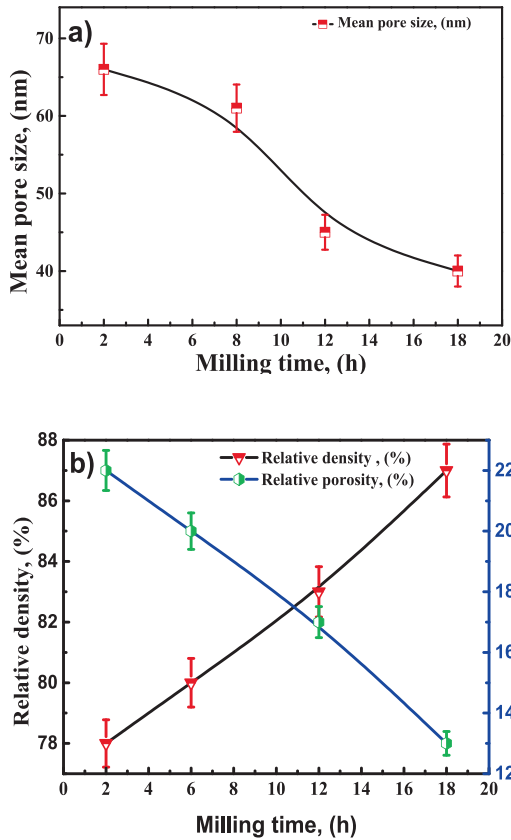
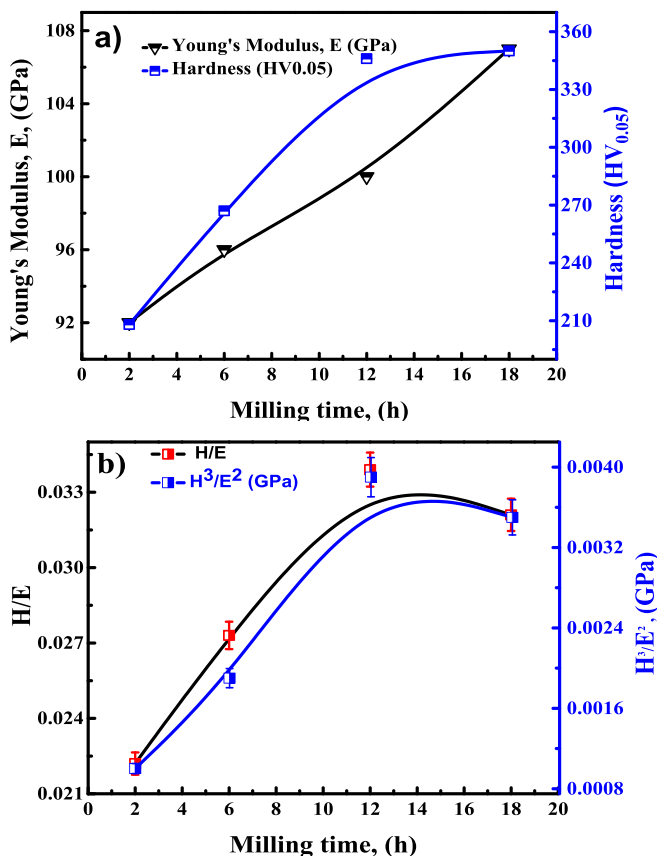**Fig. 10.** Evolution of a) mean pore size, b) Relative porosity and density of Ti-25Nb-25Zr versus milling time.

Fig. 11. Evolution of: a) Vickers hardness values and Young's modulus, b) The H/E and H^3/E^2 ratios of the milled and sintered Ti-25Nb-25Zr alloys at different milling time.
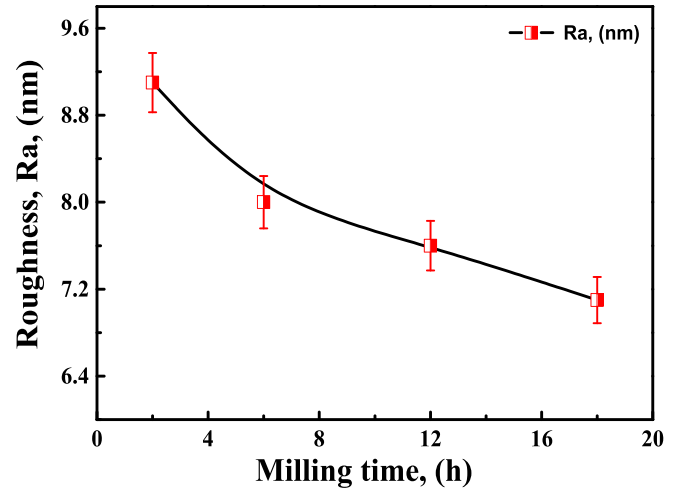

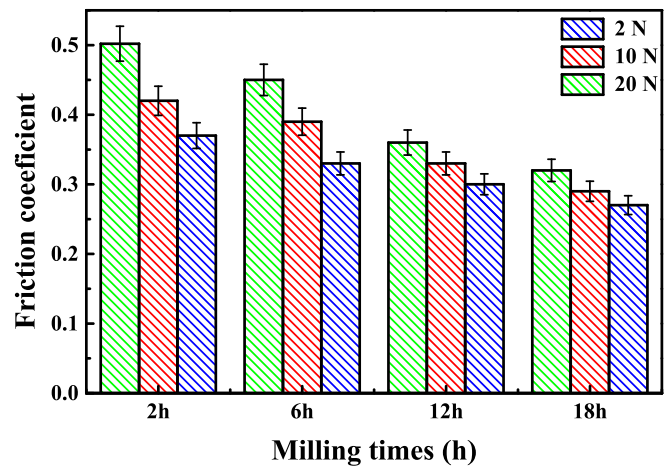**Fig. 12.** Roughness (Ra) (nm) evolution as function of milling time.

Fig. 13. Variation of friction coefficient of Ti-25Nb-25Zr alloy as function of milling time under different loads.

3.3. Tribological characterization

3.3.1. Friction and wear behavior

Fig. 13 illustrates the evolution of the average coefficient of friction of Ti25-Nb25-Zr alloys with milling times varying from 2 to 18 h at sliding speeds of 15 mm.s^{-1}.

The COF reduced from 0.502 to 0.32 with milling. As can be seen, the alloys milled at 18 h revealed lower friction coefficients compared to that milled at 2 and 6 h [52]. This is due to the oxidation activity of β-Ti alloy. The porosity causes several points of contact during the friction test. In addition, the alumina Al_2O_3-α ball can fragment the asperities, increasing the wear rate and friction coefficient [17].

The wear volume and rate evolution of Ti-25Nb-25Zr alloy are given in Fig. 14. The wear volume and wear rate tend to decrease with increasing milling time. The wear volume and wear rate of samples milled for 18 h achieve the lowest values of $9.87 \times 10^7 \mu m^3$ and $28 \times 10^{-3} \mu m^3.N^{-1}.\mu m^{-1}$, respectively. Furthermore, with an increase in applied load when the milling time is constant, the wear volume and rate of Ti-25Nb-25Zr specimens increase.

At 18 h of milling the wear volume and the wear rate varies in the range of $(9.87 \times 10^7 \mu m^3, 20.5 \times 10^7 \mu m^3)$ and $(27.67 \times 10^{-3} \mu m^3.$
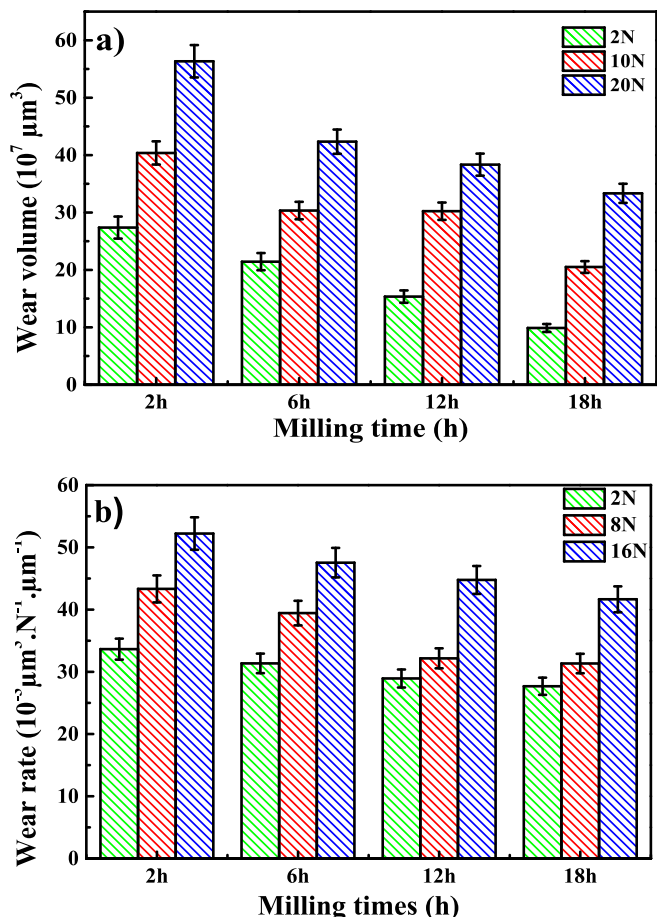
Fig. 14. Variation of: a) Wear volume and b) Wear rate of sintered Ti-25Nb-25Zr alloy.

$N^{-1}.\mu m^{-1}$, $31.33 \times 10^{-3} \mu m^3.N^{-1}.\mu m^{-1}$) for 2 N and 10 N, respectively, while at 20 N we have ($33.33 \times 10^7 \mu m^3$) and ($41.65 \times 10^{-3} \mu m^3.N^{-1}.\mu m^{-1}$), which indicates that the wear increased.

At 18 h the alloys displayed better tribological behaviour, this improved behaviour results in improved mechanical properties. The wear rate results could also be explained by strengthening mechanisms, resulting in a relatively higher rate of wear compared to other milling times of 12 and 18 h. In conclusion, biomaterials benefit from lower wear volume because it decreases the amount of metal ions released, which can cause unwanted body reactions. [53] This behaviour is influenced not only by milling time but also by their chemical composition [54].

Wear performances enhanced after 18 h milling, with a 31 % decrease in wear volume and a 19.5 % decrease in friction coefficient. The XRD analysis reveals that the presence of solely β phase in Ti-25Nb-25Zr samples has a marginal effect on reducing the wear rate due to the low hardness of these samples.

As previously mentioned, the COF and wear rates decrease as the milling times and the normal applied load increase (Figs. 13 and 14). This is caused by the improved compaction of the transfer layer that stems from increased frictional heat. Additionally, the coverage of the transfer layer increases, leading to a reduction in friction and wear rate, as previously explained [52].

3.3.2. Wear scars morphology

When a surface is subjected to applied load, various deformation mechanisms can occur depending on the magnitude of stress applied. If the stresses exceed the elastic limit of one of the two contacting materials, deformation will lead to either plasticity (ductile material) or fracture (brittle material) after a few loading cycles (elasto-plastic behavior). The evaluation of the morphology and wear marks on the milled samples and the ball enables the identification of wear mechanisms that occur during the friction of a given contact couple.

The obtained SEM micrographs highlight the surface degradation mechanisms of the samples milled at various milling times. The observations made on tracks reveal signs of both abrasive
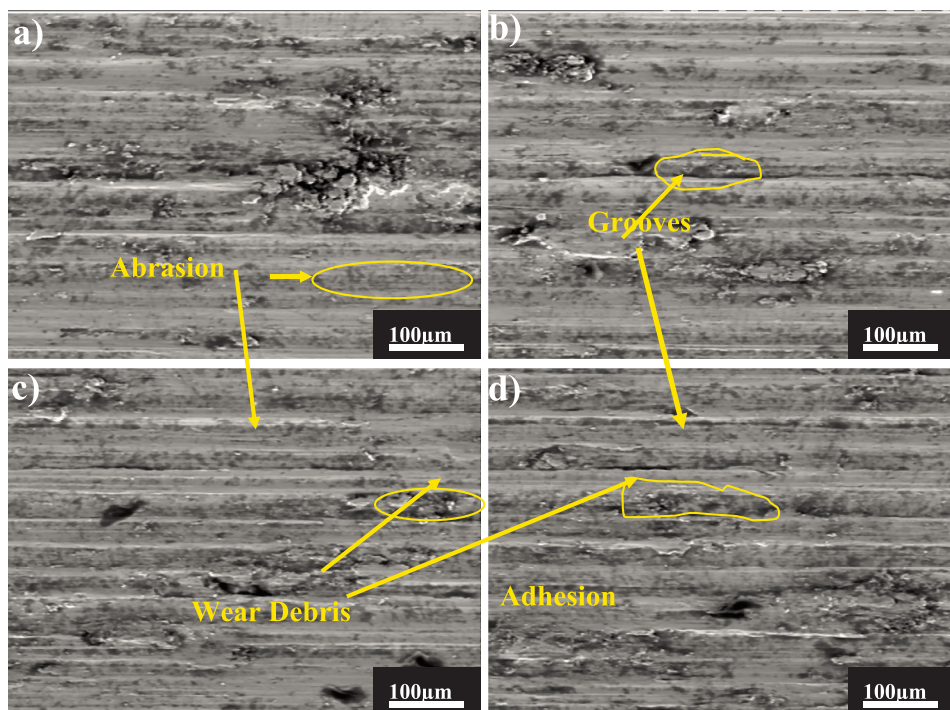

Fig. 15. SEM micrographs of wear scars morphology of the milled Ti-25Nb-25Zr alloy samples: a) – 2 h, b) – 6 h, c) – 12 and d) – 18 h.

Table 4
EDS analysis of wear scars morphology of Ti-25Nb-25Zr milled powders at different times tested at 20 N.

Milling time (h)	Ti(wt.%))	Nb(wt.%)	Zr(wt.%)	O(wt.%)	Al(wt.%)
2 h	27.5	30.6	38.4	2.3	1.5
6 h	41.6	29.3	20.7	6.4	2.05
12 h	32.2	27.8	31.2	6.5	2.3
18 h	29.1	38.6	24.4	4.7	3.2

and adhesive wear mechanisms, resulting in the presence of streaks and scratches aligned with the sliding path of the Al$_2$O$_3$ ball. These phenomena are clearly visible on worn surfaces. According to the SEM images (Fig. 15), it is apparent that there is an increase in wear debris, possibly caused by the removal of small roughness through plastic deformation or shear.

Delamination causes chips to be eliminated from the contact surface, while an adequate quantity of worn material is also removed (Fig. 15. a and b). These chips may be deposited on the alumina surface or spread across the alloy surface due to an adhesive mechanism. For the samples milled for 12 h (Fig. 14c), the streaks become deeper which could impact the tearing of the particles. These particles are generated by the rupture of asperities on the material surfaces. This normally occurs in tillage put on [41,53,54].

For the sample milled at 18 h (Fig. 15.d), scratches parallel to the path of friction were observed on the worn surfaces, indicating abrasive wear. It can be seen also signs of delamination by detachment similar to adhesive wear. These mechanisms are considered fundamental to the studied contact (Ti-25Nb-25Zr/Al$_2$O$_3$) [55–57].

Also, SEM micrograph in Fig. 15 (a-d) show that a significant amount of debris is produced, which can be attributed to the brittle nature of the Ti-Nb-Zr samples, which could be due to the alloys' fragmentation during the wear test. The amount of debris decreases with longer milling time, and the greatest amount of debris generated [36]. Table 4 shows the EDS analysis and the elements found in each sample after the tribological process. The scratching made by the alumina ball made it possible to noticeably highlight the alloying metals [18]. The proportions fluctuate depending on the scratch's depth, which in turn, depends on the hardness, resistance and milling time of each alloy.

4. Conclusions

Nanostructured Ti-25Nb-25Zr powders were successfully developed using a P7 planetary miller for 2, 6, 12 and 18 h of milling. The structural and tribological properties were investigated. The main conclusions are drawn below:

– The Ti-25Nb-25Zr particles milled for 18 h displayed ultrafine grains, and additional elements such as Zr and Nb were uniformly distributed.
– The pore size decreased with increasing milling time. The sample milled for 18 h obtained the lowest porosity of 40 nm.
– The density, hardness, and Young's modulus were increased with milling time to achieve the highest values after 18 h of milling (87 %, 350HV and 107 GPa, respectively)
– The higher wear resistance of the sample milled for 18 h is attributed to its enhanced mechanical and structural properties.
– The mechanical properties and wear behavior of the Ti-25Nb-25Zr alloy were influenced by grain size, surface roughness, and surface texture. With a longer milling time (18 h), the wear rate and the friction coefficient significantly decreased.
– The friction coefficient, wear volume and wear rate increased with increasing sliding speed and applied load.

– Due to its enhanced wear and friction resistance properties, Ti-25Nb-25Zr can be widely used in biomedical applications. The Ti-Nb-Zr alloy, after being milled for 18 h, largely satisfies the biomedical standards for implant materials.

Declaration of competing interest

The authors declare that they have no known competing financial interests or personal relationships that could have appeared to influence the work reported in this paper.

Acknowledgement

Ethical approval

None.

References

[1] M. El Khalloufi, O. Drevelle, G. Soucy, Titanium: An overview of resources and production methods, Minerals 11 (12) (2021) 1425.
[2] C. Rayane, S. Almerind, A. Agrelli, N. Andrade, Titanium dental implants: An overview of applied nanobiotechnology to improve biocompatibility and prevent infections, Materials (basel) 15 (9) (2022) 3150.
[3] M.S.E. Bougoffa, M.N. Bachir bey, C. Benouali, T. Sayah, M. Fellah, M. Abdul Samad, Dry sliding friction and wear behavior of CuZn39Pb2 and AA7075 under industrial and laboratory conditions, Journal of Bio-and Tribo-Corrosion 7 (2021) 1–17.
[4] L. Bolzoni, F. Yang, M. Jia, Effect of α+β solution treatment and aging on the performance of powder forged Ti-5Al-2.5Fe, Heat Treatment and Surface Engineering 5 (1) (2023) 2170691.
[5] S. Huang, Q. Zhao, et al., Effects of β-stabilizer elements on microstructure formation and mechanical properties of titanium alloys, J. Alloy. Compd. 876 (2021), https://doi.org/10.1016/j.jallcom.2021.160085.
[6] B. Yao, V. Kuznetsov, T. Xiao, D. Slocombe, F. Hensel, P. Edwards, Metals and non-metals in the periodic table, Philosophical Transactions: Mathematical, Physical and Engineering Sciences. 378 (2180) (2020) 213.
[7] N. Hezil, M. Fellah, Synthesis and structural and mechanical properties of nanobioceramic (α-Al2O3), J. Aust. Ceram. Soc. 55 (4) (2019) 1167–1175.
[8] S. Song, J. Tian, J. Xiao, et al., Effect of vanadium and strain rate on hot ductility of low-carbon micro alloyed steels, Metals. 12 (2022) 14.
[9] H. Demirtaş, M.A. Erden, The effect of Cr and Ni addition on mechanical properties of plain carbon steel, J. Sci. Technol. 7 (2019) 1217–1223.
[10] V.E. Bazhenov, A.V. Koltygin, V.D. Belov, Effect of iron and magnesium on alloy AL9M structure and properties, Met. Sci. Heat Treat. 59 (2017) 346–351.
[11] D. Závodská, L. Kucharíková, E. Tillová, M. Guagliano, The effect of iron content on fatigue lifetime of AlZn10Si8Mg cast alloy, Int. J. Fatigue 128 (2019) 105189.
[12] M. Farah, M. Fellah, B. Bouras, N. Hezil, A. Becheri, B. Regis, H. Daoudi, A. Montagne, A. Tmader, A.W.K. Hamiden, Unraveling the role of sintering temperature on physical, structural and tribological characteristics of ball milled Co-28Cr-6Mo biomaterial based alloy, Journal of Engineering Research (2023), https://doi.org/10.1016/j.jer.2023.10.040.
[13] M.Z. Ibrahim, A.A. Sarhan, F. Yusuf, M. Hamdi, Biomedical materials and techniques to improve the tribological, mechanical and biomedical properties of orthopedic implants–A review article, J. Alloy. Compd. 714 (2017) 636–667.

[14] A. Campos-Quirós, J.M. Cubero-Sesín, K. Edalati, Synthesis of nanostructured biomaterials by high-pressure torsion: Effect of niobium content on microstructure and mechanical properties of Ti-Nb alloys, Mater. Sci. Eng. A 795 (2020) 139972.

[15] G. Adamek, A. Junka, P. Wirstlein, M.U. Jurczyk, P. Siwak, J. Koper, J. Jakubowicz, Biomedical Ti-Nb-Zr Foams Prepared by Means of Thermal Dealloying Process and Electrochemical Modification, Materials. 15 (6) (2022) 2130.

[16] W. Xu, J. Tian, Z. Liu, X. Lu, M.D. Hayat, Y. Yan, C. Wen, Novel porous Ti-35Zr-28Nb scaffolds fabricated by powder metallurgy with excellent osteointegration ability for bone-tissue engineering applications, Mater. Sci. Eng. C 105 (2019) 110015.

[17] X.H. Yan, J. Ma, Y. Zhang, High-throughput screening for biomedical applications in a Ti-Zr-Nb alloy system through masking co-sputtering, Science China Physics. Mechanics & Astronomy. 62 (9) (2019) 1–9.

[18] M. Fellah, N. Hezil, M.Z. Touhami, M. AbdulSamad, A. Obrosov, D.O. Bokov, et al., Structural, tribological and antibacterial properties of (α+β) based Ti-alloys for biomedical applications, J. Mater. Res. Technol. 9 (6) (2020) 14061–14074.

[19] K. Pramod, G.S. Mahobia, S. Mandal, V. Singh, E. Chattopadhyay, Corrosion resistance of the surface modified Ti-13Nb-13Zr alloy by ultrasonic shot peening, Corros. Sci. 189 (2021) 109597.

[20] M. Fellah, N. Hezil, M.Z. Touhami, A. Obrosov, S. Weiß, E.B. Kashkarov, A. Iost, Enhanced structural and tribological performance of nanostructured Ti-15Nb alloy for biomedical applications, Results Phys. 15 (2019) 102767.

[21] P. Chui, R. Jing, F. Zhang, J. Li, T. Feng, Mechanical properties and corrosion behavior of β-type Ti-Zr-Nb-Mo alloys for biomedical application, J. Alloy. Compd. 842 (2020) 155693.

[22] E.D. Gonzalez, N.K. Fukumasu, C.R. Afonso, P.A. Nascente, Impact of Zr content on the nanostructure, mechanical, and tribological behaviors of β-Ti-Nb-Zr ternary alloy coatings, Thin Solid Films 721 (2021) 138565.

[23] H. Shixin, Z. Qinyang, W. Cong, L. Cheng, Z. Yongqing, J. Weiju, M. Chengliang, Effects of β-stabilizer elements on microstructure formation and mechanical properties of titanium alloys, J. Alloy. Compd. 876 (2021) 160085.

[24] M.W. Mendes, C.G. Ágreda, A.H. Bressiani, J.C. Bressiani, A new titanium based alloy Ti-27Nb-13Zr produced by powder metallurgy with biomimetic coating for use as a biomaterial, Mater. Sci. Eng. C.63 (2016) 671–677.

[25] M. Dahmani, M. Fellah, N. Hezil, M. Benoudia, A. Obrosov, S.M. Abdul, Structural and mechanical evaluation of a new Ti-25Nb-25Mo alloy produced by high-energy ball milling with variable milling time for biomedical applications, Int. J. Adv. Manuf. Technol. (2023), https://doi.org/10.1007/s00170-023-12650-0.

[26] R. Guo, G. Xiong, Tribological behavior of Ti-Al-Nb alloy with different Ta additions for high temperature applications, Mater. Lett. 300 (1) (2023) 33324.

[27] Y. Zhumagaliev, S. Baisanov, A. Chekimbaev, N. Nurgali, Phase diagram of Ti-Fe-Al system. Other Ferroalloys Fundamentals.

[28] M.O. Bodunrin, On the substitution of vanadium with iron in Ti-6Al-4V: Thermo-Calc simulation and processing map considerations for design of low-cost alloys, Mater. Sci. Eng. A 791 (2020) 139622.

[29] J. Li, S. Chen, Microstructural response and surface mechanical properties of TC6 titanium alloy subjected to laser peening with different laser energy, Opt. Laser Technol. 158 (Part A) (2023) 108836.

[30] Z.Y. Zhu, Y.L. Liu, G.Q. Gou, W. Gao, J. Chen, Effect of heat input on interfacial characterization of the butter joint of hot-rolling CP-Ti/Q235 bimetallic sheets by Laser + CMT, Sci. Rep. 11 (1) (2021) 10020, https://doi.org/10.1038/s41598-021-89343-9.

[31] Q. Zhu, J. Chen, G. Gou, H. Chen, P. Li, Ameliorated longitudinal critically refracted—Attenuation velocity method for welding residual stress measurement, J. Mater. Process. Technol. 246 (2017) 267–275, https://doi.org/10.1016/j.jmatprotec.2017.03.022.

[32] M. Dinu, S. Franchi, V. Pruna, C.M. Cotrut, V. Secchi, M. Santi, et al., Ti-Nb-Zr system and its surface biofunctionalization for biomedical applications, in: Titanium in Medical and Dental Applications, Woodhead Publishing, 2018, pp. 175–200.

[33] M.W. Mendes, C.G. Ágreda, A.H. Bressiani, J.C. Bressiani, A new titanium based alloy Ti-27Nb-13Zr produced by powder metallurgy with biomimetic coating for use as a biomaterial, Mater. Sci. Eng. C 63 (2016) 671–677.

[34] S. Changhui, L. Lisha, D. Zhengtai, L. Haoyang, Y. Fuzhen, Y. Yongqiang, L. Yueyue, Y. Jiakuo, Research progress on the design and performance of porous titanium alloy bone implants, J. Mater. Res. Technol. 3 (2023) 2626–2641.

[35] Y. Chen, S. Sun, T. Zhang, X. Zhou, S. Li, Effects of post-weld heat treatment on the microstructure and mechanical properties of laser-welded NiTi/304SS joint with Ni filler, Mater. Sci. Eng. A 771 (2020), https://doi.org/10.1016/j.msea.2019.138545 138545.

[36] M. Fellah, N. Hezil, M. Abdul Samad, R. Djellabi, A. Montagne, A. Mejias, S. Weiss, Effect of Molybdenum content on structural, mechanical, and

[37] Y. Xu, F. Zhang, W. Zhai, S. Cheng, J. Li, et al., Unraveling of Advances in 3D-Printed Polymer-Based Bone Scaffolds, Polymers 14 (3) (2022), https://doi.org/10.3390/polym14030566.

[38] Z.H. Fu, B.J. Yang, M.L. Shan, T. Li, Z.Y. Zhu, C.P. Ma, et al., Hydrogen embrittlement behavior of SUS301L-MT stainless steel laser-arc hybrid welded joint localized zones, Corros. Sci. 164 (2020) 108337, https://doi.org/10.1016/j.corsci.2019.108337.

[39] F. Hammadi, M. Fellah, N. Hezil, L. Aissani, G. Mimanne, S. Mechachti, et al., The effect of milling time on the microstructure and mechanical properties of Ti-6Al-4Fe alloys, Mater. Today Commun. 27 (2021) 102428.

[40] G. Cui, Y. Li, T. Shi, Z. Gao, N. Qiu, T. Satoh, et al., Synthesis and characterization of Eu(III) complexes of modified cellulose and poly(N-isopropylacrylamide), Carbohydr. Polym. 94 (1) (2013) 77–81, https://doi.org/10.1016/j.carbpol.2013.01.045.

[41] L. Dekhil, N. Hanneche, M. Fellah, M. Bououdina, A.M. Mercier, Structural analysis and densification study of the mechanically alloyed Cr 50 Ni 50 powders, Int. J. Adv. Manuf. Technol. 108 (2020) 2515–2524.

[42] K. Yang, H. Yu, X. Cao, J. Guan, S. Cai, Z. Yang, et al., The critical role of corrugated lamellae morphology on the tough mechanical performance of natural Syncerus caffer horn sheath, Cell Reports Physical Science (2023) 101576, https://doi.org/10.1016/j.xcrp.2023.101576.

[43] P. Sochacka, A. Miklaszewski, M. Jurczyk, Development of β-type Ti-x at. % Mo alloys by mechanical alloying and powder metallurgy: Phase evolution and mechanical properties (10≤ x≤ 35), J. Alloy. Compd. 776 (2019) 370–378.

[44] K. Yang, N. Qin, H. Yu, C. Zhou, H. Deng, W. Tian, et al., Correlating multi-scale structure characteristics to mechanical behavior of Caprinae horn sheaths, J. Mater. Res. Technol. 21 (2022) 2191–2202, https://doi.org/10.1016/j.jmrt.2022.10.044.

[45] N. Hezil, L. Aissani, M. Fellah, M.A. Samad, A. Obrosov, C. Timofei, et al., Structural, and tribological properties of nanostructured α+ β type titanium alloys for total hip, J. Mater. Res. Technol. 19 (2022) 3568–3578.

[46] M. Fellah, N. Hezil, M.A. Hussein, M.A. Samad, M.Z. Touhami, A. Montagne, S. Weiss, Preliminary investigation on the bio-tribocorrosion behavior of porous nanostructured β-type titanium based biomedical alloys, Mater. Lett. 257 (2019) 126755.

[47] J. Liu, Y. Zhou, J. Lu, R. Cai, T. Zhao, Y. Chen, et al., Injectable, tough and adhesive zwitterionic hydrogels for 3D-printed wearable strain sensors, Chem. Eng. J. 475 (2023) 146340, https://doi.org/10.1016/j.cej.2023.146340.

[48] M. Fellah, N. Hezil, L. Dekhil, M. Abdul Samad, R. Djellabi, S. Kosman, A. Montagne, A. Iost, A. Obrosov, S. Weiss, Effect of sintering temperature on structure and tribological properties of nanostructured Ti-15Mo alloy for biomedical applications, Trans. Nonferrous Met. Soc. Chin. 29 (11) (2019) 2310–2320.

[49] C. Yang, C. Yin, Y. Wu, Q. Zhou, X. Liu, Atomic insights into the deformation mechanism of an amorphous wrapped nanolamellar heterostructure and its effect on self-lubrication, J. Mater. Res. Technol. 26 (2023) 4206–4218, https://doi.org/10.1016/j.jmrt.2023.08.215.

[50] H. Guo, J. Zhang, Expansion of Sandwich Tubes With Metal Foam Core Under Axial Compression, J. Appl. Mech. 90 (5) (2023), https://doi.org/10.1115/1.4056686.

[51] N. Cui, S. Chen, T. Xu, W. Sun, B. Lv, S. Zhang, H. Niu, F. Kong, The Microstructure, Mechanical Properties, and Corrosion Resistance of a Novel Extruded Titanium Alloy, Metals. 12 (10) (2022) 1564, https://doi.org/10.3390/met12101564.

[52] M. Fellah, N. Hezil, D. Bouras, et al., Structural, mechanical and tribological performance of a nanostructured biomaterial Co-Cr-Mo alloy synthesized via mechanical alloying, J. Mater. Res. Technol. 25 (2023) 2152–2165.

[53] M. Fellah, N. Hezil, D. Bouras, A. Montagne, A. Obrosov, R. Ibrahim, A. Iqbal, El Din S, Abd El-Wahed Khalifa H. Investigating the effect of milling time on structural, mechanical and tribological properties of a nanostructured hiped alpha alumina for biomaterial applications, Arab. J. Chem. 16 (10) (2023) 105112.

[54] J. Hu, K. Yang, Q. Wang, Q.C. Zhao, Y.H. Jiang, et al., Ultra-long life fatigue behavior of a high-entropy alloy, Int. J. Fatigue 178 (2024) 108013, https://doi.org/10.1016/j.ijfatigue.2023.108013.

[55] S. Su, J. He, C. Wang, F. Gao, D. Zhong, et al., A New Dressing System Reduces the Number of Dressing Changes in the Primary Total Knee Arthroplasty: A Randomized Controlled Trial, Frontiers in Surgery 9 (2022), https://doi.org/10.3389/fsurg.2022.800850.

[56] M. Fellah, M.A. Samad, M. Labaiz, O. Assala, A. Iost, Sliding friction and wear performance of the nano-bioceramic α-Al2O3 prepared by high energy milling, Tribol. Int. 91 (2015) 151–159.

[57] B. Dikra, M. Fellah, M. Abla, B. Régis, O. Aleksei, R. Mohammed, High photocatalytic capacity of porous ceramic based powder doped with MgO, J. Korean Ceram. Soc. 60 (2023) 155–168.